Available online at www.sciencedirect.com
ScienceDirect
Polymer 47 (2006) 7131–7144
polymer
www.elsevier.com/locate/polymer

The role of clay network on macromolecular chain mobility and relaxation in isotactic polypropylene/organoclay nanocomposites

Ke Wang [a], Si Liang [a], Jinni Deng [a], Hong Yang [a], Qin Zhang [a], Qiang Fu [a,*], Xia Dong [b], Dujin Wang [b,*], Charles C. Han [b]

[a] *Department of Polymer Science and Materials, Sichuan University, State Key Laboratory of Polymer Materials Engineering, Chengdu 610065, PR China*
[b] *Key Laboratory of Engineering Plastics, Joint Laboratory of Polymer Science and Materials, Institute of Chemistry, Chinese Academy of Sciences, Beijing 100080, PR China*

Received 13 June 2006; received in revised form 24 July 2006; accepted 24 July 2006
Available online 28 August 2006

Abstract

It is well known that a so-called ''three-dimensional filler network structure'' will be constructed in the polymer/layered silicate nanocomposites when the content of layered clay reaches a threshold value, at which the silicate sheets are incapable of freely rotating, due to physical jamming and connecting of the nanodispersed layered silicate. In this article, the effect of such clay network on the mobility and relaxation of macromolecular chains in isotactic polypropylene(iPP)/organoclay nanocomposites was investigated in detail with a combination of DMTA, DSC, TGA, TEM, rheometry and melt flow index measurements. The main aim is to establish a relationship between the mesoscopic filler network structure and the macroscopic properties of the polymer nanocomposites, particularly to explore the role of the clay network on the mobility and relaxation of macromolecular chains. It was found that the nanodispersed clay tactoids and layers play less important or dominant roles on the mobility of iPP chains depending on the formation of percolating filler network. The turning point of macroscopic properties appeared at 1 wt% organoclay content. Before this point, the effect of organoclay can be negligible, and the increase of chain mobility was ascribed to the decrease of molecular weight of polymer chains, as commonly occurs during dynamic melt processing; after this point, however, a reduced mobility of chains and a retarded chain relaxation were observed and attributed to the formation of a mesoscopic filler network. The essential features of such a mesoscopic organoclay network were estimated and discussed on the basis of stress relaxation and structural reversion measurements. A schematic model was proposed to describe the different relaxation and motion behaviors of macromolecular chains in the unfilled polymer and the filled hybrids with partial and percolated organoclay networks, respectively.

Keywords: iPP/organoclay nanocomposite; Clay network; Chain mobility

1. Introduction

Recently, structure–property relationships in polymer/layered silicate nanocomposites (PLSNs) have become of interest to academia and industry [1–4]. In many previous reports, the improved properties of PLSNs, such as higher mechanical strength, enhancement of modulus, high thermal stability, low gas barrier property, increased electronic conductivity and excellent optical transparency, were commonly attributed to the structural characteristics, including the intercalated/exfoliated microstructures [5] and the good compatibility or strong interaction of layered silicate with basal polymer [1,6–9]. On the basis of investigations of the intrinsic structures of PLSNs, it was proposed that a so-called three-dimensional filler network structure will form when the content of layered clay reaches a threshold value, at which the silicate sheets are incapable of freely rotating, due to physical jamming and connecting of the nanoscale dispersed fillers [10]. The network is comprised of randomly oriented clay tactoids with locally correlated

* Corresponding authors. Tel.: +86 28 85460953; fax: +86 28 85405402 (Q.F.); tel.: +86 10 82618533; fax: +86 10 82612857 (D.W.).
E-mail addresses: qiangfu@scu.edu.cn (Q. Fu), djwang@iccas.ac.cn (D. Wang).

0032-3861/$ - see front matter © 2006 Elsevier Ltd. All rights reserved.
doi:10.1016/j.polymer.2006.07.067

layers. The dimension of filler network structure is larger than that of intercalated and exfoliated microstructures, and can be regarded as a mesoscopic structure compared to those nanoscale structures.

Since the relationships between structure and rheology were studied by Krishnamoorti and Giannelis [11,12], the melt rheological behaviors of PLSNs have been intensively ascertained. Many unusual rheological phenomena have been reported. These phenomena appear to be related to such structural features as intercalated or exfoliated microstructures, preferential orientation of anisotropic clay platelets and a mesoscopic filler network. Compared to the counterpart polymers, a pseudo-solid-like behavior in dynamic linear viscoelastic response has been found in both end-tethered (exfoliated) [12] and intercalated [13] nanocomposites. Here the independence of dynamic modulus on oscillatory shear frequency is proportional to the content of organically modified clay in the low-frequency region. In other words, the power-law relation ($G' \propto \omega^2$ and $G'' \propto \omega$) diminished gradually with increasing silicate content. The pseudo-solid-like behavior in PLSNs was ascribed to the incomplete relaxation of molecular chains upon low-amplitude strain; the incomplete relaxation originating from the geometric confinement of a percolated clay network. The non-linear viscoelastic properties of an intercalated nanocomposite of organoclay and disordered styrene–isoprene diblock copolymer were reported by Ren et al. [14,15], and a strong shear thinning effect was observed, resulting from the orientation of the silicate layers in response to the large-amplitude shear deformation. Furthermore, the disorientation kinetics was found to have non-Brownian behavior, and was independent of temperature, nanoparticle size and chemical detail, and viscoelasticity and molecular weight of the polymer matrix. In the intercalated polystyrene/clay nanocomposite, the PLSN with higher clay content exhibited much more pronounced shear thinning behavior [16,17]. Hoffmann et al. [18] demonstrated that the linear elastic modulus at low frequency of a PS/layered silicate nanocomposite with exfoliated structure was dramatically higher than that of the intercalated nanocomposite. Similarly, the homogeneously dispersed PEO/clay nanocomposite exhibited higher zero-shear-rate viscosity and sharper shear thinning tendency than the immiscible blend [19]. Contrasting to the usual shear thinning behavior in the intercalated PLSNs, a unique shear thickening (strain hardening) behavior in the end-tethered (exfoliated) PLSNs has been found by Krishnamoorti and Giannelis [20], and thought to result from the high-grafting density of polymer chains attached on the silicate surface and chain stretching beyond a critical strain amplitude in response to the applied shear. Okamoto et al. [21] attributed the strong strain-induced hardening and rheopexy features of PP/clay nanocomposite under elongational flow to the perpendicular alignment of silicate layers to the stretching direction, and a so-called ''house of cards'' structure was constructed through edge–face interactions of the silicate layers. Moreover, rheological properties could also be adopted to distinguish the degree of exfoliation [22] and monitor the morphological developments under quiescence thermal annealing [23,24] and external shear field [3,25]. For example, Lim and Park [24] demonstrated that the kinetics of intercalation in the PS/clay nanocomposite could be monitored in situ through a combination of the linear storage modulus vs. time curve and time-resolved X-ray diffraction pattern. Lele et al. [25] investigated flow-induced orientation and subsequent disorientation upon the cessation of flow in the sPP/clay nanocomposite melts through in situ rheo-X-ray diffraction measurement, which can provide direct evidence of rheology–microstructure links in such PLSNs.

Because the rheological properties of PLSN melt are highly sensitive to the essential microstructure, there exists a dramatic difference between the rheology with and without a percolating clay network. Many researchers instead propose modified models of filler networks for interpreting reasonably the unique rheological properties in PLSNs. Galgali et al. [26] suggested that the solid-like rheological response of a PP/organoclay nanocomposite originates from strong frictional interactions of the clay tactoids and sheets after formation of a percolating filler network. Within this network, the free rotation of clay tactoids is hindered by the adjacent ones. After investigating the same PLSN system, Solomon et al. [27] suggested that the hybrid network is easily destroyed by deformation, but attractive interparticle interactions would promote reconstitution of the network, giving rise to overshoot in the stress during flow reversal studies. Schmidt et al. postulated an alternative network structure formed by a dynamic adsorption/desorption equilibrium of the polymer chains onto the clay particles in the PEO/clay solution. This concept was deduced from shear-induced viscoelastic response [28] and orientation behaviors [29] of such solutions which have been probed by rheometry, flow-birefringence and small-angle neutron scattering (SANS). Other novel filler network models have also been proposed recently in EVA copolymer/organoclay hybrids [30,31], copolyamide/organoclay nanocomposites [32], epoxy based PLSN [33], polyamide/fibrous clay nanocomposite [34], and even in a PEO/silica nanocomposite [35] and a system of PMMA and single-walled carbon nanotubes [36].

The physically associated filler network in a polymer-based nanocomposite should also have a significant effect on the ultimate properties of nanocomposites. Only a few studies have been concerned with structure–property relationships and the essential role of the filler network on the dynamic behavior of macromolecular chains [35–38]. To our knowledge, a correlation between a mesoscopic filler network and macroscopic properties is crucial for designing high performance polymer materials and for their processing, but this has rarely been a concern in the past investigations.

In the current study, we focused our attention mainly on the relationship between the mesoscopic filler network and the macroscopic properties, such as melt fluidity, crystallization capability and thermogravimetric behavior in the intercalated iPP/montmorillonite nanocomposites [39]. The trend of the macroscopic properties was found to correspond well with the melt rheological properties as a function of clay content. Our results demonstrate that a competition between shear-induced degradation of macromolecules and a formation of

a physically combined clay network is responsible for the significant dependence of macroscopic properties on the content of organically modified montmorillonite. A critical point of macroscopic properties appeared at 1 wt% organoclay content. Before this point, the macroscopic properties were mostly dependent on increased chain mobility that can be ascribed to the scission of polymer chains commonly occurred in the dynamic melt processing. After this point, the melt rheological properties begin to exhibit a pseudo-solid-like behavior, indicating the initiation of filler network formation. Consequently, the motion of iPP chains is restricted within the mesoscopic filler network, resulting in a significant transition in the development of macroscopic properties. Based on the results of transmission electron microscopy (TEM), dynamic mechanical thermal analysis (DMTA) and melt rheometry, a mechanism is suggested that the mobility and relaxation of macromolecular chains are retarded by the geometric confinement of the organoclay network. The effects of the physically connected clay network structure on the structural reversibility of as-prepared iPP/OMMT hybrids against applied shear deformation were also studied. Finally, a schematic model is proposed to represent the different relaxation and motion behaviors of macromolecular chains in the unfilled polymer and in the filled composites with partial and percolated organoclay networks, respectively.

2. Experimental

2.1. Materials

A commercially available isotactic polypropylene (trade marked as T30S, Yan Shan Petroleum China) with $M_\eta = 29.2 \times 10^4$ g/mol, melt flow index (MFI) of 3.07 g/10 min (230 °C, 2.16 kg) and density of 0.91 g/m^3 was used as the basal resin. The compatibilizer, PP grafted maleic anhydride (PP-*g*-MA) (MA content = 0.9 wt%, MFI = 6.74 g/min at 190°C), in which maleic anhydride group is randomly grafted on a PP backbone, was purchased from Chen Guang Co. (Sichuan, China). Sodium montmorillonite (MMT) with a cation exchange capacity (CEC) of 68.8 mmol/100 g (RenShou, Sichuan, China) was organically modified through ion-exchanged reaction with dioctadecyl dimethylammonium bromide. The ion-exchange procedure can be found in our previous publication [40]. Although the CEC of MMT seems to be low, the *d*-spacing of intergallery has been prominently improved from 1.4 nm for raw MMT to 3.4 nm after ion-exchanging, indicating a good availability of such MMT for organic modification. Hereafter, the organically modified MMT is abbreviated as OMMT.

2.2. Preparation of iPP/OMMT nanocomposites

Master-batch pellets with a composition of iPP/PP-*g*-MA/OMMT (80/20/20 wt%) were firstly melt-mixed in a TSSJ-2S co-rotating twin-screw extruder. The temperature of the extruder was maintained at 170, 180, 190, 200, 200 and 195 °C from hopper to die, and the screw speed was about 110 rev/min. Then a series of iPP/PP-*g*-MA/OMMT nanocomposites (90/10/*x* wt%, $x = 0.5$, 1, 2, 3, 5) were obtained through adding iPP and PP-*g*-MA to dilute the as-prepared master-batch in the extruder. This material is hereafter abbreviated as iPP/OMMT. An unfilled iPP/PP-*g*-MA (90/10 wt%) blend was simultaneously prepared for comparison.

2.3. Measurements and characterization

2.3.1. Transmission electron microscope (TEM)

Transmission electron microscopic observations (TEM) were carried out to examine the micro-morphology of the samples. Ultra-thin sections of the specimens were cut from the extruded pellets perpendicular to the flow direction using a Reichert Ultracut-S ultramicrotome equipped with a FCS cryodevice. The thin slices were put on copper grids and then submitted to TEM observations on a JEM-2010 TEM under an acceleration voltage of 200 kV.

2.3.2. Dynamic mechanical thermal analysis (DMTA)

Dynamic mechanical properties of as-prepared iPP/OMMT nanocomposites were measured using a dynamic mechanical thermal analyzer (DMTA V, Rheometric Scientific Ltd. UK) in the tensile mode with a strain of 0.02%. The temperature range was between −50 and 150 °C with a heating rate of 5 °C/min. The frequency used was 1.0 Hz. The size (length × width × thickness) of the test samples was $10 \times 7 \times 0.3$ mm^3.

2.3.3. Differential scanning calorimetry (DSC)

A Perkin–Elmer DSC-7 was used to determine the influence of OMMT content on the crystallization behavior of the as-prepared nanocomposites. The test samples (about 5 mg) were first heated to 200 °C at a heating rate of 10 °C/min and then held at 200 °C for 5 min to eliminate the thermal history. The cooling curves were recorded from 200 °C to room temperature at a cooling rate of 10 °C/min. All measurements were conducted under a nitrogen atmosphere.

2.3.4. Thermogravimetric analysis (TGA)

Thermogravimetric analysis was carried out on a Perkin–Elmer thermogravimetric analyzer (TGA-7). The test samples (about 2 mg) were heated under a nitrogen atmosphere from ambient temperature up to 650 °C at a heating rate of 20 °C/min.

2.3.5. Melt flow index

A Haake SWO 556-0031 Meltflixer (Polymertechnik GmbH) was used to estimate the melt fluid behavior of as-prepared hybrids. All the experiments were conducted under a constant temperature of 230 °C and an invariable imposed pressure of 2.16 kgf. The melt fluid indexes were gained after averaging at least 15 values.

2.3.6. Melt rheology

All rheological measurements were performed on a controlled strain rheometer (ARES rheometer, Rheometrics Scientific, NJ) with a torque transducer range of 0.2–2000 gf cm

using 2.5 cm diameter parallel plates at 190 °C. Testing sample disks with a thickness of 1.5 mm and a diameter of 2.5 mm were prepared by compression molding of the extruded pellets at 190 °C for 3 min. Small-amplitude oscillatory shear measurements were conducted within a frequency range of 0.01–100 rad/s. A sinusoidal strain of the form

$$\gamma(t) = \gamma_0 \sin(\omega t)$$

where γ_0 is strain amplitude, ω is oscillatory frequency and t is time, was imposed on the testing samples. Stress-relaxation experiments were conducted under low (10%) and large (200%) strains. A single-step strain γ was applied at time = 0, and the shear stress $\sigma(t)$ was measured as a function of time. Structural recovery experiments were conducted according to the following procedure: (1) the initial storage modulus ($G'(0)$) was detected under low-amplitude oscillatory shear mode (shear frequency = 1 rad/s, strain = 1%); (2) a steady shear deformation (shear rate = 2 s^{-1}) was exerted on the testing samples at an interval of 600 s; (3) the linear storage modulus ($G'(t)$) was recorded again as a function of quiescent time under the same conditions in step (1), and the G' at plateau (G'(equi)) was also examined at the end of structural recovery. Moreover, the required time from the cessation of shear to the equilibrium of structural recovery, t_{equi}, could also be extracted from step (3) for the estimation of restricted kinetics of iPP chain motion and relaxation during structural disorientation. For ensuring the reliability of rheological data, trace antioxidant has been added into composites during melt extrusion and all rheological measurements were conducted under nitrogen atmosphere to minimize oxidative degradation of the polymer.

3. Results

3.1. The mesoscopic clay network

It has been well established that an intercalated/exfoliated structure is usually formed in iPP/OMMT system by using PP-*g*-MA as compatibilizer [1,4]. However, the formation of a clay network depends on the connecting of clay layers and tactoids. For the purpose of this study, we present our data by first examining the dispersion of clay in the as-prepared nanocomposites as a function of clay content (Fig. 1). In these TEM pictures, some aggregations of OMMT tactoids are also

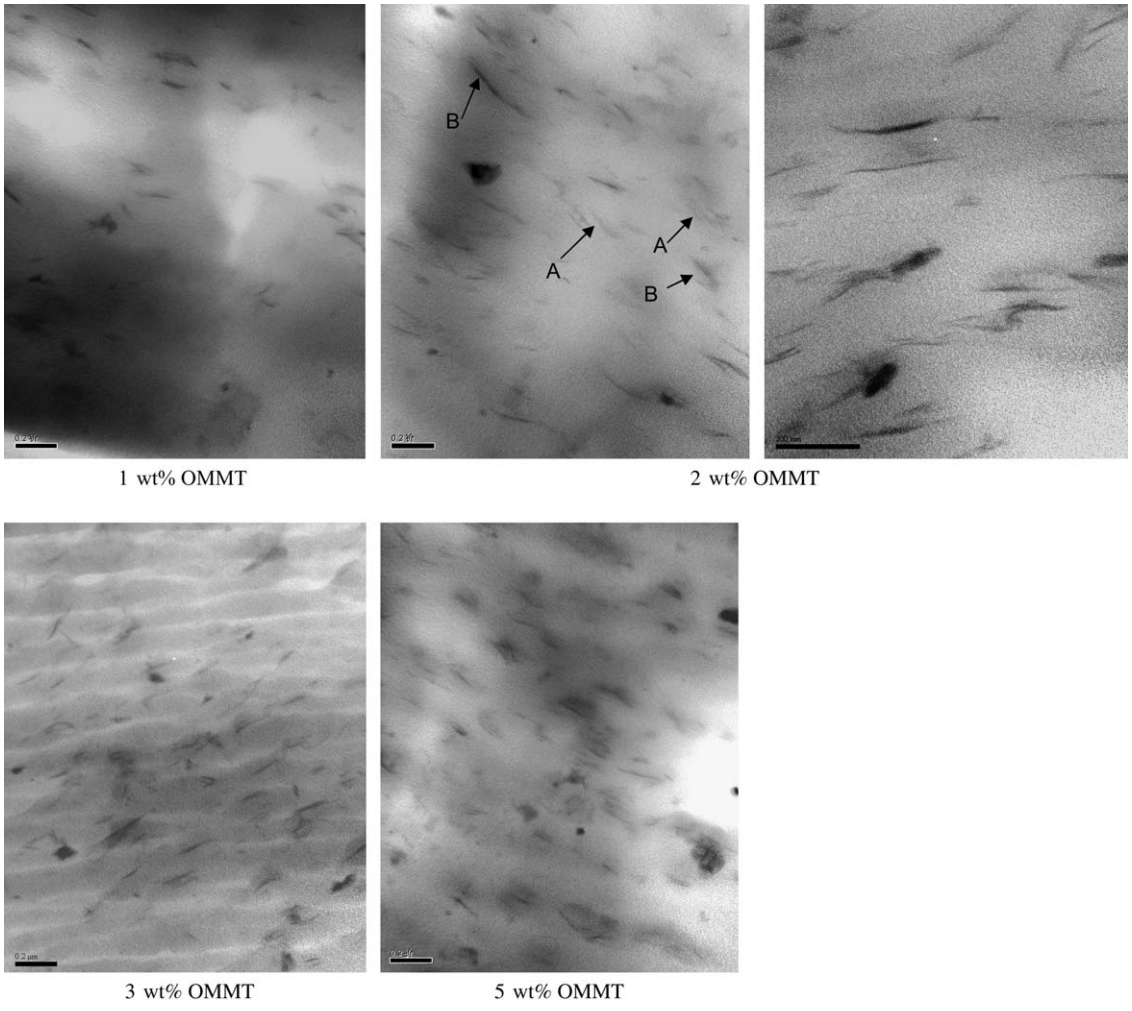

Fig. 1. TEM images of the as-prepared iPP/OMMT nanocomposites with various OMMT contents. Inside the pictures, A indicates individual OMMT layers and B tactoids. For clear observation, the representative image with high magnification at 2 wt% content is also presented (scale bar = 200 nm).

detectable, which indicate that the exfoliation degree in such polyolefin/OMMT nanocomposites synthesized via melt compounding is lower than the polar polymer/clay systems, such as nylon/clay [41], PMMA/clay [42], epoxy/clay [43] nanocomposites, in which well-defined exfoliations of clay were frequently approved by WAXD and TEM proofs. It can be ascribed to the fact that the chemical miscibility and interaction between PP chains and OMMT particles are still weak compared to the polar polymer-based nanocomposites even if the compatibilizer with weak polarity is incorporated. The modification of chemical miscibility between PP and OMMT is very limited through addition of PP-*g*-MA. A qualitative analysis of the internal structures in iPP/OMMT composites can be drawn through direct visualization. The geometric sizes of layered OMMT particles are roughly estimated through the representative TEM image with high magnification at 2 wt% content. Multiple scaled OMMT structures are observed in composites, among which intercalated and partially exfoliated OMMT domains dominate, with tactoid thickness of tens of nanometers, length of less than 200 nm and individual layer thickness of several nanometers and length of 100 nm. So a broaden dispersion of aspect ratio of layered OMMT particles is around 40–80. Moreover, according to our previous work [39], the mean *d*-spacing of intercalated tactoids is about 4.1 nm ($2\theta = 2.3^\circ$), whereas the quantitative estimation of exfoliated domains would be relied on means of small-angle X-ray diffraction and needs further investigations. It should be noted that the exfoliated degree in polyolefin/organoclay system is independent of the content of organoclay [39], which results in the dominant intercalated structure even if the clay content is low (1 wt%). Increasing the OMMT content seems to enhance the density of clay tactoids and layers in the PP matrix, resulting in a decrease of the ratio of the averaged spacing between neighboring particles to the average length of tactoids and layers. This will lead to gradual formation of spatially linked structure of dispersed OMMT tactoids and layers in PP matrix, and ultimately to a ''percolating filler network structure'' as the clay content reaches a certain threshold.

The existence of such percolated filler network was often ignored in many literatures about PLSNs, because it was difficult to probe and discover the intrinsic features of filler network only depending on morphologic investigations. However, as suggested by Krishnamoorti and Silva [10], the relaxation kinetics of polymer chains is prominently restricted after the formation of mesoscopic clay network. Dynamic melt rheometry is a powerful means to inspect the effect of inorganic filler on the motion and relaxation of polymer chains. In our study, the construction of a mesoscopic clay network will be further demonstrated by the change of dynamic melt rheological properties of the studied materials. The storage modulus G' and loss modulus G'' under small-amplitude oscillatory shear are shown in Fig. 2a and b, respectively. In the high ω regime corresponded to the movement within small timescale, not much difference of the G' is seen for the composites with various OMMT contents (0–5 wt%), which implied that the movements of partial polymer chains, such as segments and methyl groups tethered on the backbone, were unaffected by OMMT nanoparticles. However, the G' in the low ω regime is significantly dependent on the OMMT content, i.e., the G' of nanocomposites is slightly lower than that of basal polymer when the OMMT content is lower than 2 wt%. On the contrary, the G' at high OMMT concentration is higher than that of base polymer. The rheological properties in the low ω regime can be regarded to reflect the relaxation and motion of whole PP chains. The frequency-independence of G' in the low-frequency regime, regarded as a pseudo-solid-like behavior that the terminal slope of $G'-\omega$ curve approaches zero, does not increase monotonically with increasing OMMT content until a threshold content is reached, at $\sim$2 wt% OMMT. The terminal slope of $G'-\omega$ curves begins to decrease when the OMMT content reaches 2 wt% indicating that there are adequate number of layered OMMT particles to establish a percolated filler network in which the free movement of PP chains is restricted by the spatially confined geometry, resulting in the incomplete relaxation of the chains upon the applied small-amplitude strain over a long time range. Similarly, in the case of end-tethered nylon/layered silicate nanocomposite [12], the $G'-\omega$ curve within low-frequency regime at 2 wt% clay content is significantly deviated from the curve of pure nylon. Obviously, the extent of restricted relaxation should be proportional to the OMMT content as described by the schematic illustrations in the left of Fig. 2a. Therefore the increasing OMMT content will induce the gradual decrease of terminal slope of $G' \sim \omega$ curve. However, the difference of modulus dependence on frequency at terminal region is less when OMMT content is lower than 3 wt%, and it is difficult to confirm that the threshold content relied merely on rheometry. While the beginning formation of percolated clay network at 2 wt% OMMT content will be approved through monitoring the developed trend of macroscopic properties as increasing of OMMT content in the next section. The terminal slopes of G'' vs. ω curves are approximately comparable for the iPP/OMMT composites over the full OMMT concentration range (Fig. 2b). The increase in the frictional stress, which originates from the difference in the relative motion between silicate particles and basal resin, is limited, even though the percolating filler network has been constructed at high concentration.

Sequentially, the elucidation of melt rheological properties is correlated to morphological observation through spatial TEM analysis. The dispersed morphology of OMMT particles has been spatially resolved at 5 wt% content, at which the connection level between silicate fillers is highest according to the melt rheological measurement. The TEM images in two orthogonal planes (N–T and N–R planes) of parallel-plate rheological cell are shown in Fig. 3. As illustrated by the inset sketch, N, T and R represent the normal, tangential and radial directions, respectively. In the N–T plane perpendicular to the radial direction, the layered OMMT tactoids and sheets are randomly dispersed and many physical jamming sites between adjacent nanoparticles are observed, suggesting the establishment of mesoscopic filler network; while, in the N–R plane parallel to the radial direction, the ordering degree of

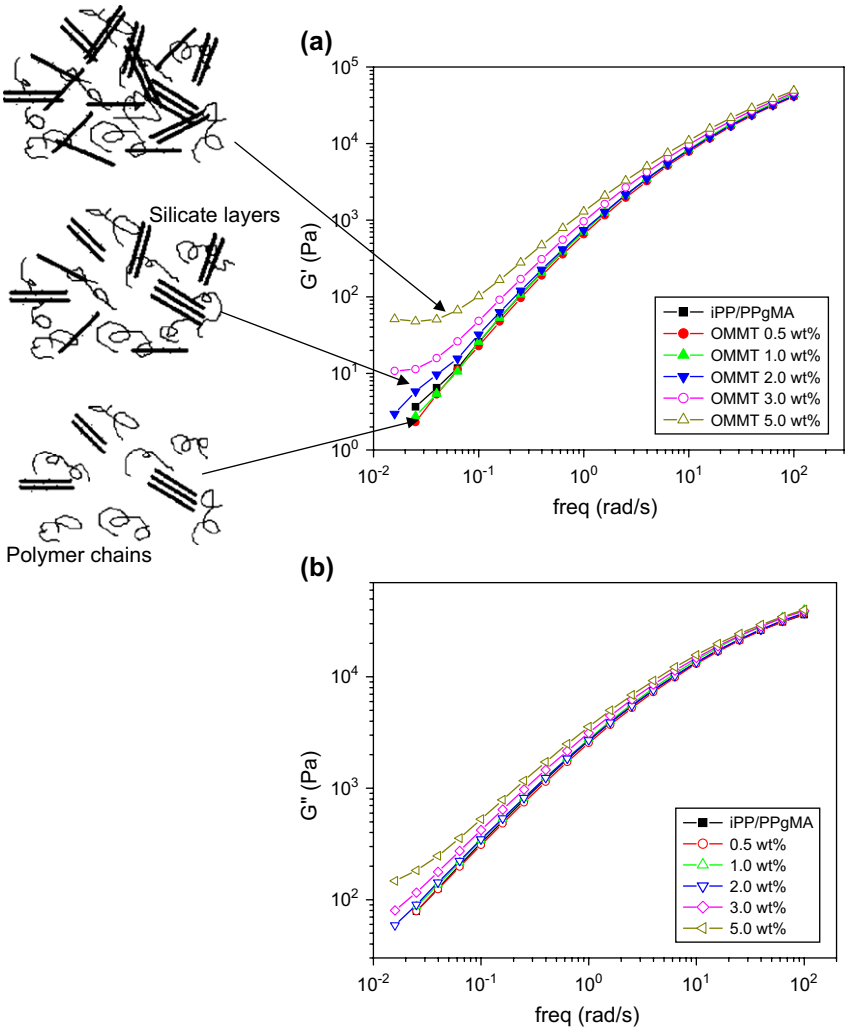

Fig. 2. Linear melt-state rheological properties as a function of oscillatory frequency: (a) storage modulus, G' and (b) loss modulus, G''.

arrangement of OMMT particles seems to be higher than that in another plane and a medium preferential orientation of OMMT along the radial direction is detected, which could be attributed to the effect of compression molding of rheological testing specimens.

3.2. Macroscopic properties

As demonstrated above, a percolated clay network composed with layered OMMT particles will be constructed after a threshold content of OMMT was reached. A schematic

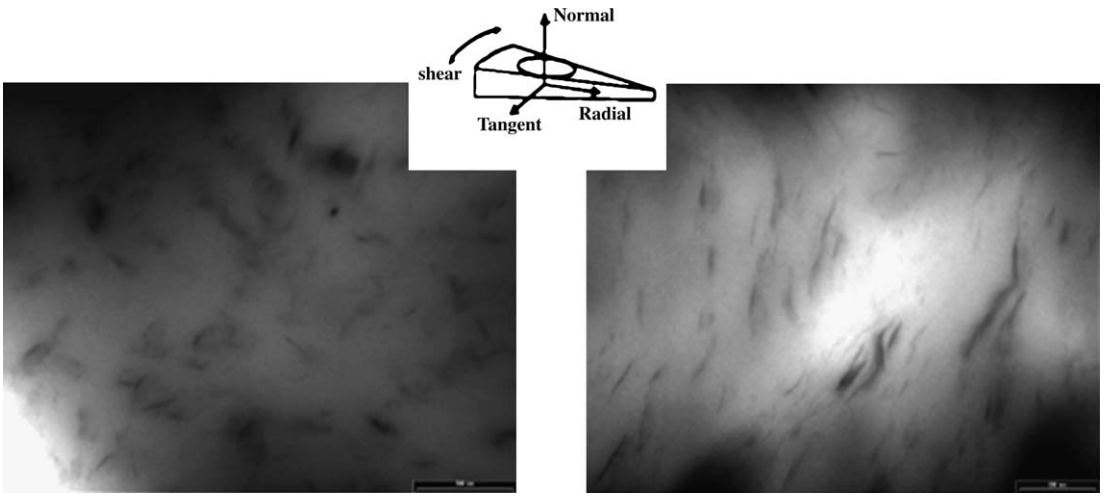

Fig. 3. TEM images demonstrate the OMMT morphologies in two orthogonal planes of parallel-plate rheological cell. The OMMT content is 5 wt%.

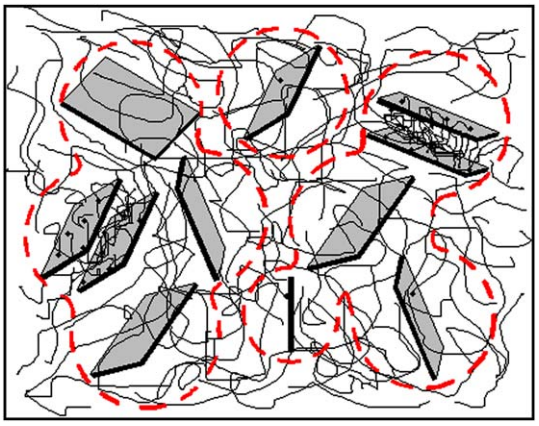

Fig. 4. Schematic illustration of the physical jamming of clay particles and the restricted motion of PP chains within the 3D percolated clay network.

illustration describing the internal structure in such clay network is shown in Fig. 4, in which the free tumbling of OMMT sheets is incapable because many trace circles of tumbling are overlapped with each other, and the motion and relaxation of PP chains will be hindered by the confined geometry originated from the layered clay particles. Obviously, the mesoscopic clay network will affect the macroscopic properties through retarded motion of PP chains. The macroscopic properties of iPP/clay nanocomposites investigated in our study include melt flow index, non-isothermal crystallization temperature, thermal degradation temperature and dynamic mechanical thermal analysis. The measurement of melt flow index (MFI) is a simple yet very useful way to estimate the chain mobility of polymer materials (Fig. 5). It is valuable to note that the addition of nanodispersed OMMT at low content (<2 wt%) can improve the melt fluidity, while after the OMMT content reaches a value of threshold of percolating network (2 wt%), the fluidity of melt hybrids is depressed by the clay loading, similar to the conventional MFI variation in polymer/inorganic filler composites. The formation of clay network is the reason for the change of MFI as the increase of OMMT content. It can be conceived that the orientation and flow of PP chains would be retarded if the

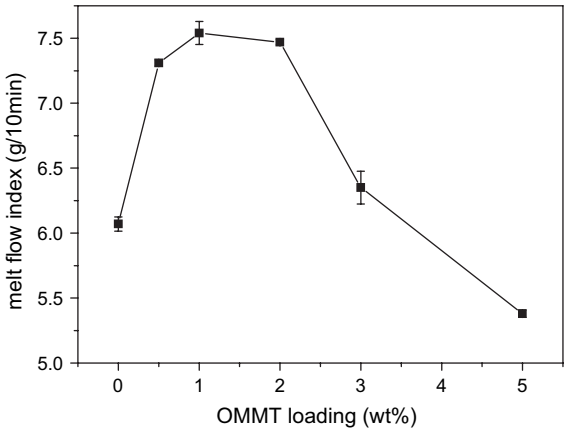

Fig. 5. Effect of OMMT content on the melt fluidity (melt flow index, MFI) of as-prepared iPP/OMMT nanocomposites.

PP chains were confined in narrow spacing between clay particles, resulting in the decrease of melt fluidity. The observed tendency of MFI is consistent with linear rheological behavior.

As a common expectation, the nanodispersed OMMT particles can act as nucleating agents and facilitate the crystallization process of nanocomposite, resulting in a higher crystallization temperature (T_c). Nevertheless, the crystallization capability of nanocomposite will not be monotonically improved through the addition of a large amount of organoclay if the filler network plays a role to restrict the movement of molecular chains. This statement is confirmed by Fig. 6, which shows DSC cooling crystallization curves of as-prepared iPP/OMMT nanocomposites. The crystallization temperature first increases with the addition of OMMT, but then decreases as the clay content exceeds 1 wt%, although in this case the crystallization temperatures of nanocomposites are still higher than that of basal polymer. Such a phenomenon was also reported in the literature [44]. However, in the instance of nylon 6/clay nanocomposite, it was reported that the organic surfactant attached on the OMMT sheets could disturb the hydrogen bonding of nylon 6 chains and thus affect the crystallization kinetics of nylon 6. But in our study, the crystallization behavior is simplified in that only few factors including OMMT particles as nucleating agent, PP molecular weight and confined motion of PP chains within clay network are considered. After all, the concentration of polar maleic anhydride is low in our iPP/OMMT nanocomposites and could be ignored. The thermal stability of iPP/organoclay nanocomposites behaves with a trend similar to that of the crystallization temperature (Fig. 7). The thermal degradation temperatures of the nanocomposites at lower OMMT content (0.5 and 1 wt%) are lower than that of basal polymer, while after the formation of a mesoscopic filler network (OMMT content ≧ 2 wt%) the thermal stability is obviously reinforced with the addition of higher amount of organoclay.

The macroscopic properties of the iPP/OMMT nanocomposite were further investigated by dynamic mechanical thermal analysis. As shown in Fig. 8a, the transition peak of loss modulus G'' representing the glass–rubber transition of iPP chains shifts to a low temperature with the increase of OMMT content, suggesting a higher degree of molecular chain mobility. Quantitatively, the T_g decreases from 10 °C for the base iPP to −15 °C for the iPP/OMMT nanocomposite (5 wt% OMMT). The existence of the mesoscopic filler network is reflected by the variation of storage modulus G' (Fig. 8b). Within the temperature range from −50 to 20 °C, a decreased storage modulus can be obtained as the clay content is lower than 2 wt%, caused by the increased degree of molecular chain mobility. However, a jump of storage modulus occurs as the content reaches to 2 wt%, due to the formation of a clay network. We can observe a two-step decrease of the storage modulus for the composites with high clay content (above 1 wt%). A sharp decrease of G' around −25 °C is due to the glass transition, and a consequent slight increase at ca. 25 °C is observed, corresponding to the characteristic behavior of the mesoscopic filler network structure. Recently in the polyurethane/polyhedral oligomeric silsesquioxane (POSS) nanocomposite incorporating a high content

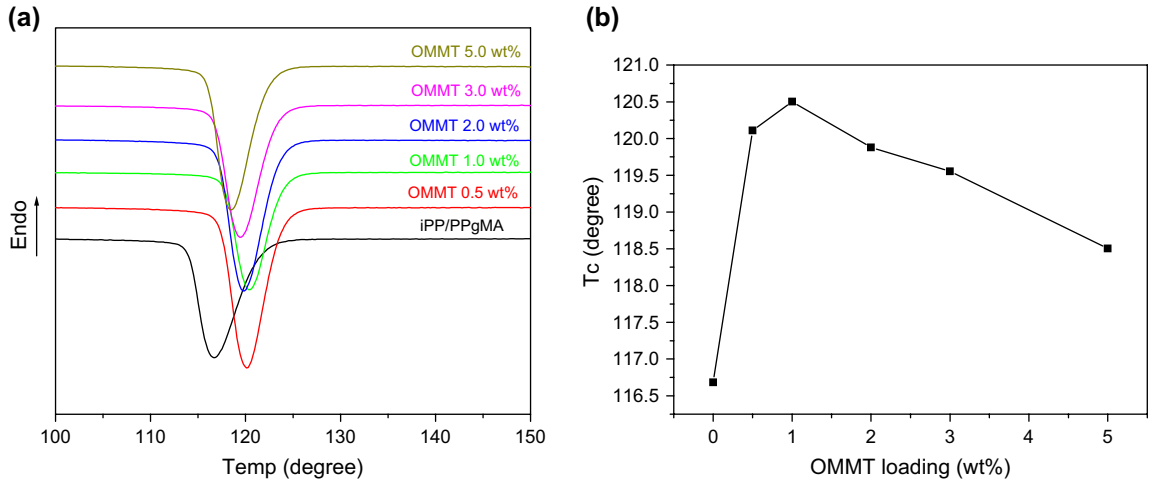

Fig. 6. (a) DSC cooling crystallization thermograms of as-prepared iPP/OMMT nanocomposites and (b) cooling crystallization temperatures (T_c) of as-prepared iPP/OMMT nanocomposites as a function of OMMT content. The datum in (b) is extracted from (a) and consistent with the peak values of cooling crystallization curves.

of POSS, an added high-temperature transition peak in the tan δ vs. temperature spectrum has been reported, which is ascribed to the nanoreinforcement effect of the POSS cages [45]. Our present conclusion is in good agreement with the above report.

4. Discussion

4.1. Different roles of nanodispersed OMMT before and after the formation of mesoscopic filler network

In order to interpret the unique property variation of iPP/OMMT nanocomposite, including melt fluidity, crystallization habit, thermal stability as well as storage modulus with OMMT content, it is very important to identify what kind of roles the nanodispersed OMMT tactoids and layers play on the mobility of iPP chains before and after the establishment of a percolated filler network. As has been discussed before, the loss modulus G'' of as-prepared nanocomposites is weakly influenced by the addition of OMMT (Fig. 2b), implying that the impact of OMMT on the interfacial interaction and frictional stress between iPP/organophilic silicate is relatively weak, compared to that of the conventional inorganic filler. Therefore, the effect of OMMT nanoplatelets on the restricted motion of iPP chain can be neglected before the formation of percolated clay network. So, what is the internal reason that the mobility of iPP chains is increased at low OMMT content (1 wt%)? In a recent report [46], a plasticizing function of the chains of alkyl ammonium used as the surfactant of organically modified filler has been proposed. Obviously, such plasticizing function can be responsible for the promoted mobility of polymer chains. Otherwise, the scission of macromolecular chains occurring commonly in the molten compounding process can, of course, promote the mobility of polymer chains. Especially, our composites are prepared through a two-step process as described in the experimental section. In this way different extents of scission of PP and PP-*g*-MA chains could

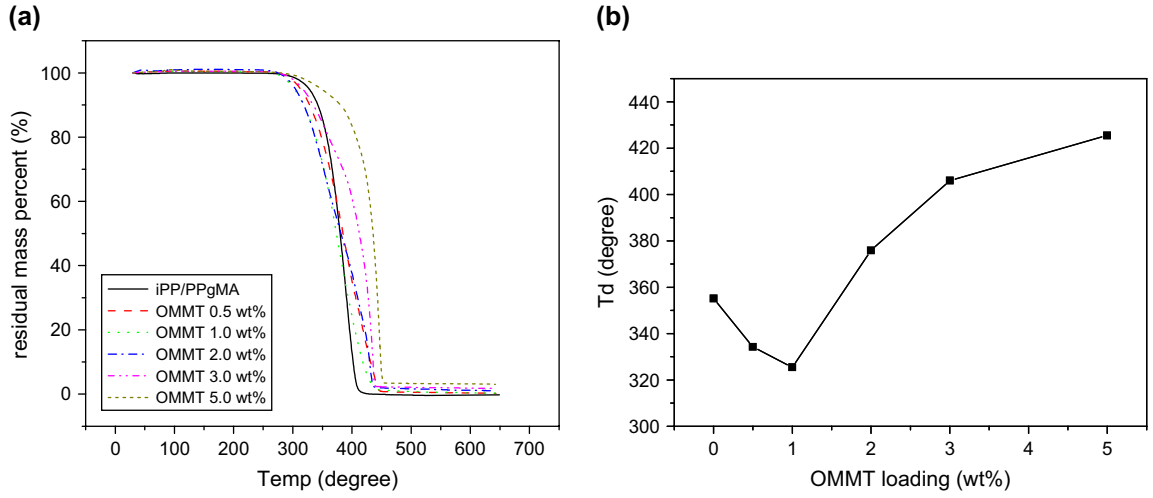

Fig. 7. (a) TGA curves of iPP/OMMT hybrids containing various OMMT contents and (b) thermal degradation temperatures (T_d) as a function of OMMT content. The datum in (b) is extracted from (a) and corresponded to the values at largest slope of TGA curves.

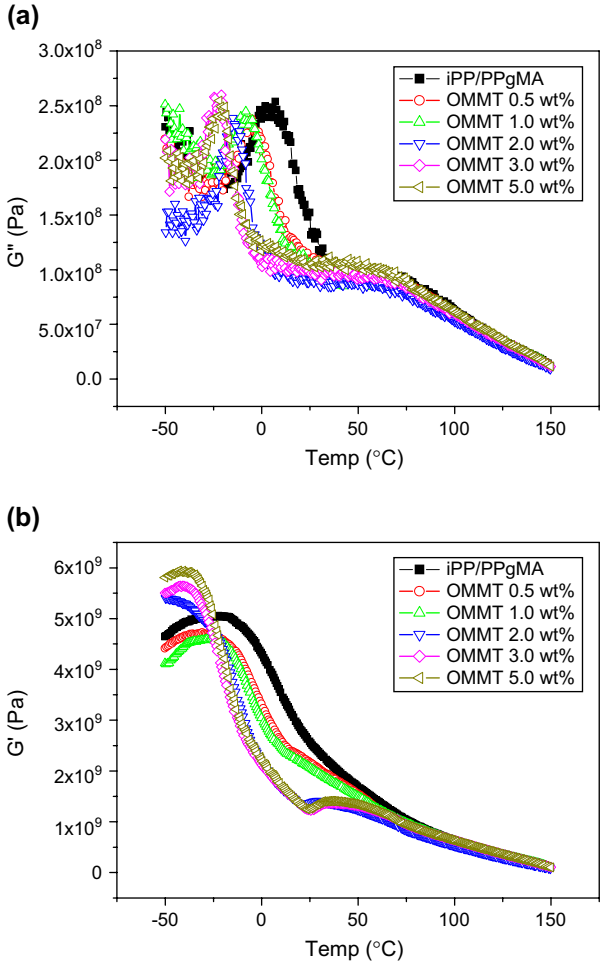

Fig. 8. Dynamic mechanical properties of iPP/OMMT nanocomposites containing various OMMT contents as a function of temperature: (a) G'' and (b) G'.

be induced in the composites with different OMMT contents, because the numbers of master-batch experienced twice melt extrusion in various composites are different to each other. So the scission extent of molecular chains as a function of OMMT content is unexpected and the molecular weight evidence is necessary for consideration the chain mobility. The molecular weight decrease of iPP in iPP/OMMT composite after two-step melt extrusion is evidently proved by GPC data (Table 1). The organoclay in the testing solutions has been filtered before the GPC measurements. According to the molecular weight evidence, however, we would rather take account of the scission of macromolecular chains as the intrinsic cause of promotion of chain mobility at low OMMT content. Adding organically modified clay can cause an obvious weight-mean molecular weight decrease of iPP by 50%, which is generally considered relate to the impact of the organic modifier, dioctadecyldimethyl ammonium. When the OMMT concentration lies in the range of 0–1 wt%, M_w decreases monotonically, consistent with the changing tendency of macroscopic properties, suggesting that the increasing mobility of iPP chains plays a dominant role in determining the ultimate properties of as-prepared composites.

As the OMMT content continuously increases and exceeds 1 wt% in the iPP/OMMT composite, however, the MFI values decrease with increasing OMMT content, with the related average molecular weight decreasing slightly. All corresponding macroscopic properties of the composite show the same turning point around OMMT concentration 1 wt%. The reason is that as OMMT content exceeds 1 wt%, the nanodispersed clay tactoids/sheets progressively establish and complete the mesoscopic network structure. It is conceivable that the mobility and relaxation of iPP chains will be confined by the physically correlated cage comprising layered OMMT tactoids and layers, resulting in the opposite evolution of macroscopic properties after the threshold (1 wt%) of filler content. So, in contrast to the cases of low OMMT content, the role of a percolated filler network created at high OMMT content is dominant in determining the macroscopic properties, resulting in low melt fluidity, retarded crystallization capability, and an enhanced thermal stability and modulus. In summary, the competition between the scission of macromolecular chains and the establishment of a filler network of percolated clay that activates and retards the motion of iPP chains, respectively, is responsible for the existence of turning point in the development of macroscopic properties in iPP/OMMT composites.

4.2. Mechanism of retarded motion and relaxation of iPP chains within a mesoscopic organoclay network

If the cages of inorganic fillers hinder the motion and relaxation of iPP chains, a retarded stress-relaxation behavior like in pseudo-solid materials is desired in the as-prepared nanocomposite melts. The stress-relaxation behaviors of unfilled iPP and iPP/OMMT composites in the linear viscoelastic regime (strain = 10%) and non-linear viscoelastic regime (strain = 200%) are presented in Fig. 10. The adopted strain amplitudes, 10% and 200%, are according to the strain response spectra (Fig. 9). In such stress-relaxation experiments, a single-step strain was imposed on the melt at time = 0, and the shear stress $\sigma(t)$ was recorded immediately as a function of time. Within the testing strain range from 0.05% to 300%, the melt stress is linearly increased with strain amplitude, therefore the magnitude of stress at large strain (non-linear regime) is considerably larger than that at small strain (linear regime).

Table 1
Molecular weight characteristics of iPP/OMMT composites prepared via melt extrusion

OMMT content	0 wt%	0.5 wt%	1.0 wt%	2.0 wt%	3.0 wt%	5.0 wt%
M_w	2.27×10^5	1.49×10^5	1.16×10^5	1.30×10^5	1.26×10^5	1.17×10^5
M_n	0.78×10^5	0.54×10^5	0.47×10^5	0.50×10^5	0.48×10^5	0.45×10^5
M_w/M_n	2.92	2.75	2.44	2.59	2.70	2.61

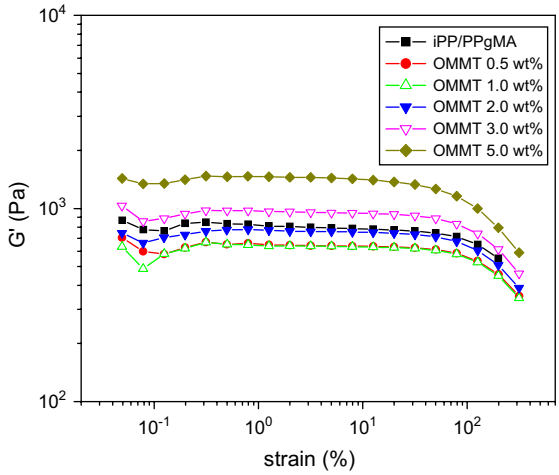

Fig. 9. Melt storage modulus vs. strain curves as a function of OMMT content.

Interestingly, in the linear strain regime (Fig. 10a), the stress relaxation of the unfilled polymer and iPP/OMMT composites is independent of the OMMT content; i.e., the stress of all the investigated samples decreases linearly with time. When the stress-relaxation measurements were conducted in the non-linear regime (Fig. 10b), a slow stress-relaxation phenomenon is observed in the iPP/OMMT composite with 5 wt% OMMT, in which the highest degree of mesoscopic filler network is expected. Such stress relaxation in our iPP/OMMT nanocomposites is quite different from what has been reported in PS–PI diblock copolymer/layered silicate nanocomposites [13,14]. From the above traditional stress-relaxation experiments, we come to the tentative conclusion that the organoclay network confines the chain motion and relaxation of iPP. In order to further understand the essential mechanism of the confined motion of iPP chains within a physically associated clay network, we designed a novel rheological method, and the results will be addressed below.

Restricted relaxation of polymeric chains within the adjacent domain of layered silicate has been confirmed in epoxy/clay composites [47], but the essential mechanism is still uncertain, not to mention in the non-polar polyolefin/organoclay nanocomposites with the mesoscopic filler network structure. On the basis of the structural recovery measurements, we now propose an interpretation for the retarded motion of iPP chains due to their confinement within a percolated organoclay network. Here the iPP/OMMT (3 wt%) composite is taken as an example (Fig. 11). A steady shear deformation (shear rate $= 2\ s^{-1}$, time $= 600$ s) was exerted on the melt, which forced the macromolecular chains and clay sheets to align parallel to the direction of shear stress. The initial connections, including entanglement between molecular chains and electrostatic attraction of organoclay tactoids/sheets, will be disturbed and destroyed during the shear deformation process. In the following step, the disorientation of aligned iPP chains and the reconstruction of an equilibrium structure in the composite were monitored in real-time by a rheometer under the small-amplitude oscillatory mode (strain $= 1\%$). After cessation of shear, the time-dependent storage modulus, $G'(t)$, was recorded immediately. It is observed in Fig. 11(3) that $G'(t)$ increases gradually with quiescent time until a plateau value, G'(equi), is reached, which implies that a novel equilibrium structure upon the steady shear deformation has been established. The structural recovery spectra ($G'(t)/G'$(equi)) of the iPP/OMMT composites are plotted in Fig. 12 and the values of structural reversion time, t_{equi}, are also listed in this figure. It should be emphasized that the various curves in Fig. 12 represent the same process that has been demonstrated in Fig. 11(3) and the ratio of ($G'(t)/G'$(equi)) as ordinate parameter is for normalizing unity under different OMMT contents. The magnitude of t_{equi} represents qualitatively the impeded kinetics of structural recovery and relaxation; for example, if the mobility of iPP chains is restricted within geometric confinement of a filler network, a longer t_{equi} is expected and its value is strongly dependent on the perfection of the filler network structure. Although the unfilled iPP has the highest molecular weight, its t_{equi} cannot be detected, possibly due to the quick reversion rate of molecular chains.

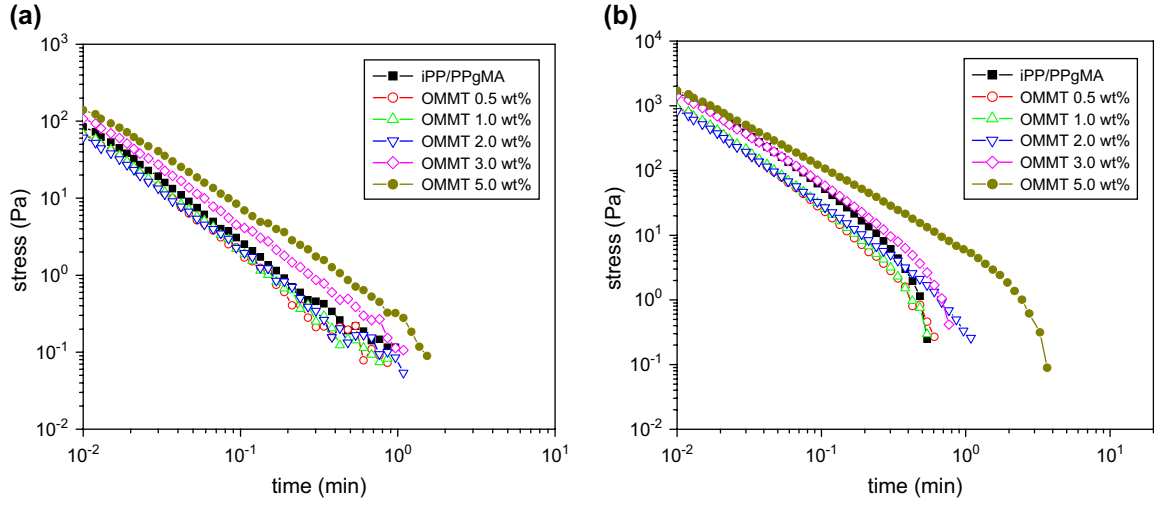

Fig. 10. Stress-relaxation spectra of compatiblized iPP/OMMT hybrids under (a) low-amplitude strain (10%) and (b) large-amplitude strain (200%).

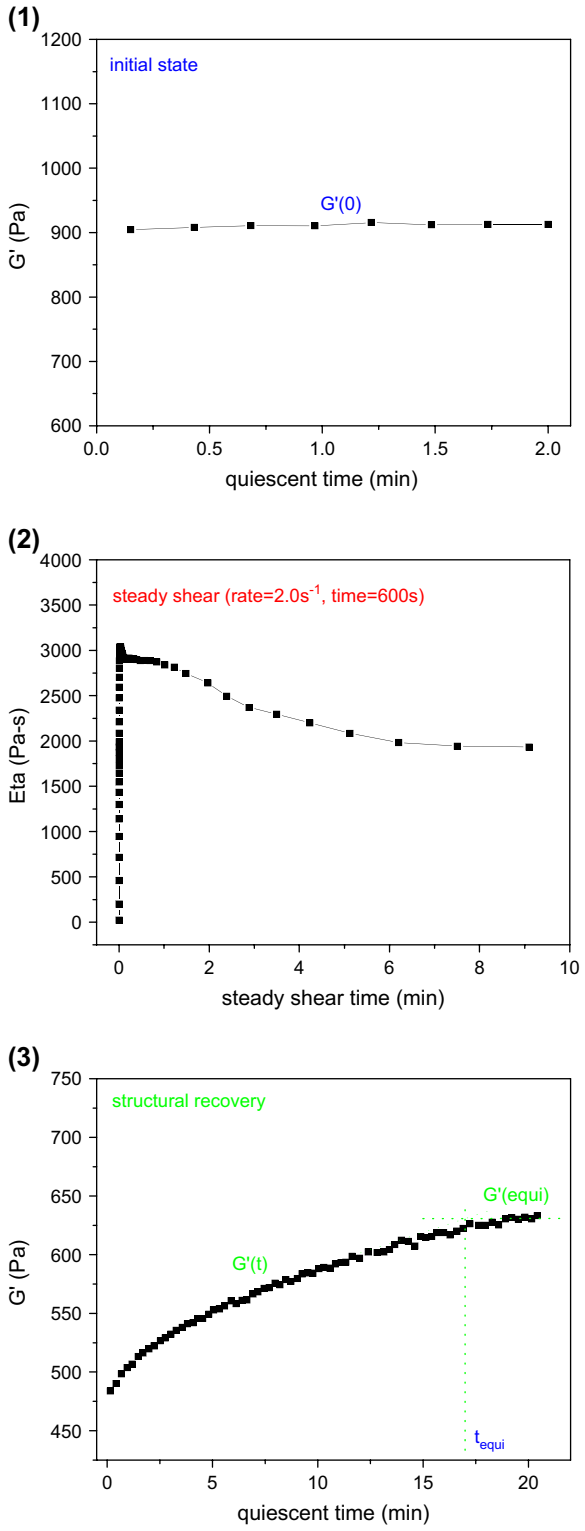

Fig. 11. The protocol of structural reversion experiments as that (1) the initial storage modulus ($G'(0)$) was detected under low-amplitude oscillatory shear mode (shear frequency = 1 rad/s, strain = 1%); (2) a steady shear deformation (shear rate = 2 s^{-1}) was exerted on the testing samples for a interval of 600 s; (3) the linear storage modulus ($G'(t)$) was recorded again as a function of time under the same conditions in step (1), and the G' at equilibrium ($G'(\text{equi})$) was also examined at the end of structural recovery.

The iPP/OMMT nanocomposites, however, show slower structural recovery, ranging from 2.2 min for iPP/OMMT 0.5 wt% to 29.7 min for iPP/OMMT 5 wt%, suggesting that the disorientation and relaxation of aligned iPP chains and OMMT layers are independent of the molecular weight of iPP, but rather determined by OMMT content. In other words, the mobility of iPP chains is depressed by the formation of a percolated clay network.

It has been generally accepted that an electrostatic attraction exists between positively charged edges and negatively charged faces of silicate sheets [10,37]. When the amount of silicate sheets per unit volume exceeds a threshold value of physical correlation, the individual sheets will connect with each other through such electrostatic attraction. It is reasonable that the interaction between silicate layers is gradually reinforced with increasing OMMT content once the percolation of filler network structure begins. Unlike a polar polymer/organoclay system, where the molecular chains with polar end groups will tether to the surfaces of clay platelets and the platelets can be regarded as the physical cross-link points, the force between non-polar chain and organoclay is very weak in polyolefin/organoclay composites. So the structural recovery in these nanocomposites should be dominated by the OMMT content. The effect of OMMT content on the structural reversibility of iPP/OMMT composites has been manifested in Fig. 13, where the ratio $G'(\text{equi})/G'(0)$ vs. OMMT loading is plotted. The value of $G'(\text{equi})/G'(0)$ is remarkably improved from 0.35 for the unfilled polymer to 0.73 for iPP/OMMT 5 wt%. We can now explain why the reversibility of the linear elastic property is intimately related to the OMMT content. When the percolating filler network structure has been established, the internal structural features of the macromolecular assembly, such as the entanglement of iPP chains, can be effectively maintained upon applied steady shear deformation. On the contrary, the initial assembly of macromolecular chains in the unfilled polymer can be destroyed thoroughly by external shear deformation and the following structural recovery becomes very difficult. So, the degree of elastic modulus recovery is improved as the perfection of the organoclay network.

To understand the mechanism of the retarded relaxation and mobility of iPP chains within the filler network, a schematic illustration is proposed (Fig. 14). Two distinct characteristics of structural reversion of iPP/OMMT nanocomposites with physically connected clay network have been taken into account: (1) the retarded mobility and relaxed kinetics of the oriented structure and (2) the high degree of structural reversibility. In the case of unfilled polymer, the physical entanglement between iPP chains decreases and the iPP chains align parallel to each other upon steady shear deformation. After releasing shear, the iPP chains will quickly relax back into individual coils, resulting in a remarkable decrease in linear elastic modulus. So, the relaxed structure of unfilled iPP (individual coils) is quite different from the initial structure of macromolecular assembly (entanglement). For composites with lower clay content, before the establishment of a percolated filler network, the connection between iPP chains will

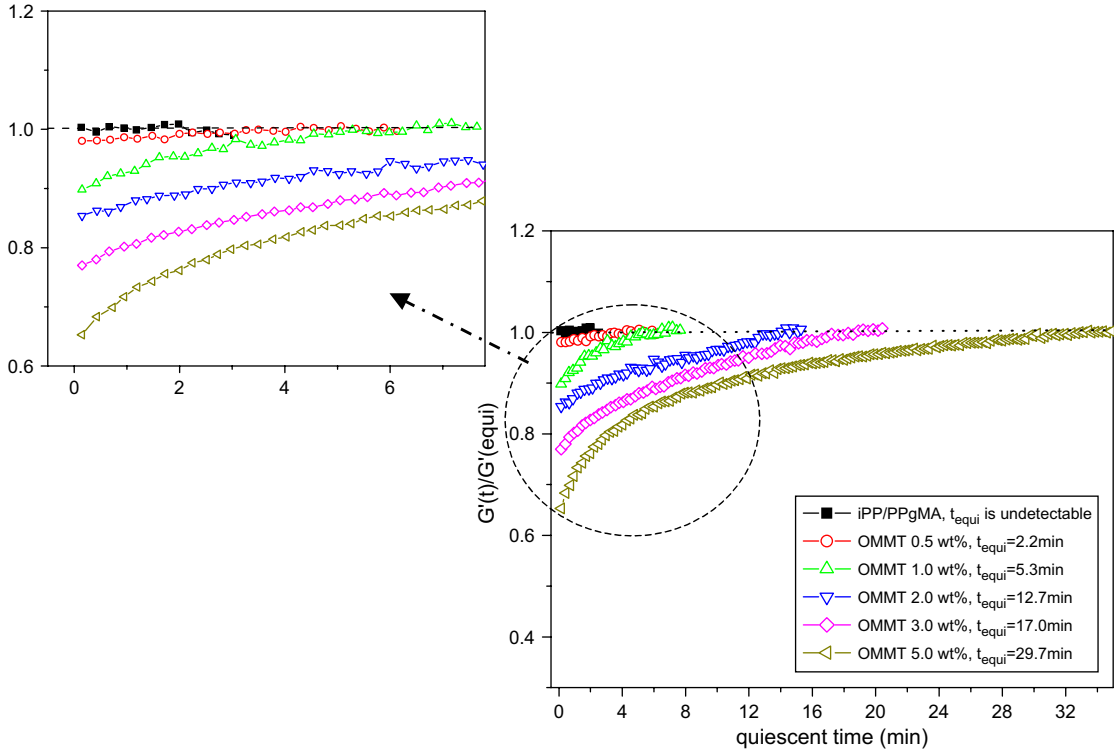

Fig. 12. Structural reversion spectra ($G'(t)/G'$(equi) vs. time curves) as a function of OMMT content. Inset shows enlarged initial portion of the same curves for clarity.

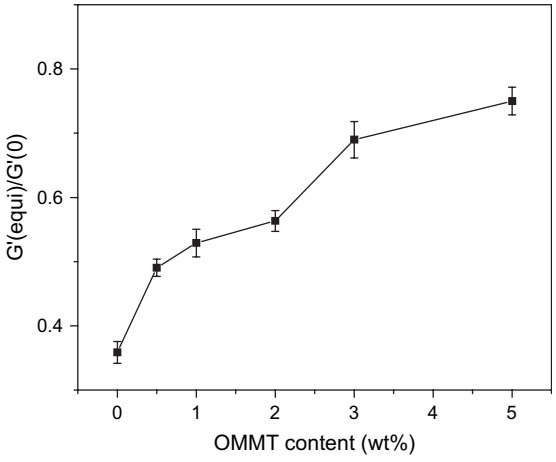

Fig. 13. The effect of OMMT content on the structural reversibility of as-prepared nanocomposites (the ratios of G'(equi)/G'(0)).

be partially maintained because of the physical conjunction provided by the pairs of face-to-face OMMT platelets, resulting in the slow relaxation rate of oriented iPP chains and partial improvement of structural reversibility. A cooperative motion of iPP chains under the steady shear deformation will take place after the formation of mesoscopic filler network and the connection between iPP chains is almost undisturbed because of the strong conjunction among OMMT platelets. So the initial structure of the macromolecular assembly is recoverable easily and the motion of iPP chains is retarded. The confined motion of macromolecular chains in the mesoscopic filler network is believed to be helpful for improving the durability and size stability of polymer/clay nanocomposites. Further investigation on the properties of solid-state iPP/OMMT composites is undergoing in our laboratory.

5. Conclusions

The correlation between the mesoscopic filler network structure and the macroscopic properties in iPP/OMMT nanocomposites has been systematically investigated in this work. It is identified that the impact of nanodispersed OMMT tactoids and layers on the mobility of iPP chains is weak before the construction of a percolated filler network, which is dominant in determining the macroscopic properties of investigated composites. Once such a percolated filler network is formed, the role of the molecular weight of iPP becomes unimportant, while the filler network determines the macroscopic properties of the composites, leading to low melt fluidity, retarded crystalline capability and enhanced thermal stability and modulus. The essential features of the confined motion of iPP chains within such mesoscopic filler network have been investigated through melt stress relaxation and structural reversion characterization. It is postulated that the percolated filler network induces cooperative motion of iPP chains through the conjunction of OMMT sheets with iPP chains, resulting in retarded relaxation of the oriented structure and improved structural reversibility of iPP/OMMT nanocomposites.

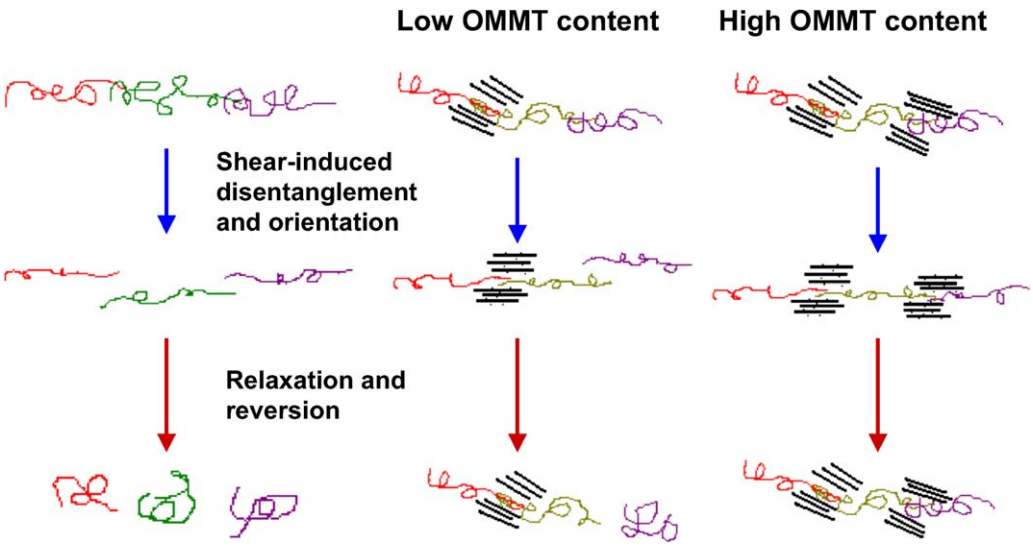

Fig. 14. Schematic representations of different modes of iPP chain relaxation and motion behaviors in the unfilled polymer and the filled hybrids with partial and percolated organoclay networks, respectively.

Acknowledgments

We would like to express our great thanks to the National Natural Science Foundation of China (50533050, 20490220, 20574081 and 50290090) for financial support. This work was subsidized by the special funds for Major State Basic Research Projects of China (2003CB615600). This work was also supported by the Ministry of Education of China.

References

[1] Ray SS, Okamoto M. Prog Polym Sci 2003;28:1539.
[2] Kuila BK, Nandi AK. Macromolecules 2004;37:8577.
[3] Ray SS, Okamoto K, Okamoto M. Macromolecules 2003;36:2355.
[4] (a) Kawasumi M, Hasegawa N, Kato M, Usuki A, Okada A. Macromolecules 1997;30:6333;
(b) Nam PH, Maiti P, Okamoto M, Kotaka T, Hasegawa N, Usuki A. Polymer 2001;42:9633;
(c) Yu YH, Yeh JM, Liou SJ, Chang YP. Acta Mater 2004;52:475.
[5] (a) Nathani H, Dasari A, Misra R. Acta Mater 2004;52:3217;
(b) Vaia R, Jandt KD, Kramer EJ, Giannelis EP. Chem Mater 1996;8:2628.
[6] Marchant D, Jayaraman K. Ind Eng Chem Res 2002;41:6402.
[7] Wang K, Chen L, Wu J, Toh ML, He C, Yee AF. Macromolecules 2005;38:788.
[8] Tseng CR, Wu JY, Lee HY, Chang FC. Polymer 2001;42:10063.
[9] Shah D, Maiti P, Jiang DD, Batt CA, Giannelis EP. Adv Mater 2005;17:525.
[10] Krishnamoorti R, Silva AS. In: Pinnavaia TJ, Brall GW, editors. Polymer–clay nanocomposites. New York: John Wiley & Sons; 2000. p. 315–43.
[11] Krishnamoorti R, Vaia RA, Giannelis EP. Chem Mater 1996;8:1728.
[12] Krishnamoorti R, Giannelis EP. Macromolecules 1997;30:4097.
[13] Ren J, Silva AS, Krishnamoorti R. Macromolecules 2000;33:3739.
[14] Ren J, Krishnamoorti R. Macromolecules 2003;36:4443.
[15] Ren J, Casanueva BF, Mitchell CA, Krishnamoorti R. Macromolecules 2003;36:4188.
[16] Kim TH, Jang LW, Lee DC, Choi HJ, Jhon M. Macromol Rapid Commun 2002;23:191.
[17] Zhong Y, Zhu Z, Wang SQ. Polymer 2005;46:3006.
[18] Hoffmann B, Dietrich C, Thomann R, Friedrich C, Mulhaupt R. Macromol Rapid Commun 2000;21:57.
[19] Choi HJ, Kim SG, Hyun YH, Jhon MS. Macromol Rapid Commun 2001;22:320.
[20] Krishnamoorti R, Giannelis EP. Langmuir 2001;17:1448.
[21] Okamoto M, Nam PH, Maiti P, Kotaka T, Hasegawa N, Usuki A. Nano Lett 2001;1:295.
[22] Wagener R, Reisinger T. Polymer 2003;44:7513.
[23] Lee JA, Kontopoulou M, Parent JS. Polymer 2004;45:6595.
[24] Lim YT, Park O. Macromol Rapid Commun 2000;21:231.
[25] Lele A, Mackley M, Galgali G, Ramesh C. J Rheol 2002;46:1091.
[26] Galgali G, Ramesh C, Lele A. Macromolecules 2001;34:852.
[27] Solomon MJ, Almusallam A, Seefeldt K, Somwangthanaroj A, Varadan P. Macromolecules 2001;34:1864.
[28] (a) Schmidt G, Nakatani AI, Han CC. Rheol Acta 2002;41:45;
(b) Lin-Gibson S, Kim H, Schmidt G, Han CC, Hobbie EK. J Colloid Interface Sci 2004;274:515.
[29] (a) Schmidt G, Nakatani AI, Batler PD, Karim A, Han CC. Macromolecules 2000;33:7219;
(b) Schmidt G, Nakatani AI, Batler PD, Han CC. Macromolecules 2002;35:4725;
(c) Gibson SL, Schmidt G, Kim H, Han CC, Hobbie EK. J Chem Phys 2003;119:8080.
[30] Gelfer MY, Burger C, Chu B, Hsiao BS, Drozdov AD, Si M, et al. Macromolecules 2005;38:3765.
[31] Prasad R, Pasanovic-Zujo V, Gupta RK, Cser F, Bhattacharya SN. Polym Eng Sci 2004;44:1220.
[32] Incarnato L, Scarfato P, Scatteia L, Acierno D. Polymer 2004;45:3487.
[33] Dean D, Walker R, Theodore M, Hampton E, Nyairo E. Polymer 2005;46:3014.
[34] Shen L, Lin Y, Du Q, Zhong W, Yang Y. Polymer 2005;46:5758.
[35] Zhang Q, Archer LA. Langmuir 2002;18:10435.
[36] Du F, Scogna RC, Zhou W, Brand S, Fischer JE, Winey KI. Macromolecules 2004;37:9048.
[37] Haraguchi K, Li HJ, Matsuda K, Takehisa Toru, Elliott E. Macromolecules 2005;38:3482.
[38] Koo CM, Kim JH, Wang KH, Chung IJ. J Polym Sci Part B Polym Phys 2004;43:158.
[39] Wang K, Liang S, Zhang Q, Du R, Fu Q. J Polym Sci Part B Polym Phys 2005;43:2005.

[40] (a) Zhang Q, Fu Q, Jiang L, Lei Y. Polym Int 2000;49:1561;
(b) Zhang Q, Wang K, Men Y, Fu Q. Chin J Polym Sci 2003;21:359.
[41] (a) Fornes TD, Yoon PJ, Keskkula H, Paul DR. Polymer 2001;42: 9929;
(b) Fornes TD, Yoon PJ, Hunter DL, Keskkula H, Paul DR. Polymer 2002;43:5915.
[42] (a) Su S, Wilkie CA. J Polym Sci Part B Polym Phys 2003;41:1124;
(b) Okamoto M, Morita S, Kim YH, Kotaka T, Tateyama H. Polymer 2001;42:1201.
[43] (a) Chin IJ, Albrecht T, Kim HC, Wang J. Polymer 2001;42:5947;
(b) Kong D, Park CH. Chem Mater 2003;15:419;
(c) Lu JK, Ke YC, Qi ZN, Yi XS. J Polym Sci Part B Polym Phys 2001; 39:115.
[44] Liu X, Wu Q. Polymer 2001;42:10013.
[45] Liu HZ, Zheng S. Macromol Rapid Commun 2005;26:196.
[46] Chen X, Yoon K, Burger C, Sics I, Fang D, Hsiao B, et al. Macromolecules 2005;38:883.
[47] Lu H, Nutt S. Macromolecules 2003;36:4010.